Article

TRANSPARENT PROCESS

THE EMBO JOURNAL

Oct4-induced oligodendrocyte progenitor cells enhance functional recovery in spinal cord injury model

Jeong Beom Kim[1,2,*], Hyunah Lee[1,2], Marcos J Araúzo-Bravo[3,4], Kyujin Hwang[5], Donggyu Nam[1,2], Myung Rae Park[1,2], Holm Zaehres[6], Kook In Park[5] & Seok-Jin Lee[1,2]

Abstract

The generation of patient-specific oligodendrocyte progenitor cells (OPCs) holds great potential as an expandable cell source for cell replacement therapy as well as drug screening in spinal cord injury or demyelinating diseases. Here, we demonstrate that induced OPCs (iOPCs) can be directly derived from adult mouse fibroblasts by Oct4-mediated direct reprogramming, using anchorage-independent growth to ensure high purity. Homogeneous iOPCs exhibit typical small-bipolar morphology, maintain their self-renewal capacity and OPC marker expression for more than 31 passages, share high similarity in the global gene expression profile to wild-type OPCs, and give rise to mature oligodendrocytes and astrocytes *in vitro* and *in vivo*. Notably, transplanted iOPCs contribute to functional recovery in a spinal cord injury (SCI) model without tumor formation. This study provides a simple strategy to generate functional self-renewing iOPCs and yields insights for the in-depth study of demyelination and regenerative medicine.

Keywords direct conversion; myelination; *Oct4*; oligodendrocyte progenitor cell; self-renewal

Subject Categories Neuroscience; Stem Cells

DOI 10.15252/embj.201592652 | Received 23 July 2015 | Revised 14 September 2015 | Accepted 17 September 2015 | Published online 23 October 2015

The EMBO Journal (2015) 34: 2971–2983

Introduction

Oligodendrocyte progenitor cells (OPCs) are originated from the neuroepithelium during embryonic development (Noll & Miller, 1993). OPCs are a bipotent glial cell type in the central nervous system (CNS) that can differentiate into both astrocytes and myelinogenic oligodendrocytes, responsible for forming myelin sheath (Franklin & Ffrench-Constant, 2008) that insulates axons for the efficient propagation of action potentials (Najm *et al*, 2011). Demyelinating conditions, such as traumatic spinal cord injury (SCI), cause immediate cell damage, which can subsequently lead to both motor and sensory dysfunctions that result in devastating paralysis (Lee *et al*, 2014). Since there are no full restorative treatments yet available and current strategies including surgical interventions and medications carry severe side effects (Silva *et al*, 2014), cell replacement therapy by transplanting neural/glial progenitors (Ben-Hur & Goldman, 2008; Jin *et al*, 2011) for restoration of demyelinated lesions is a promising treatment option. In particular, transplantation of oligodendrocytes or OPCs derived from pluripotent stem cells promotes axonal remyelination and facilitates functional recovery of the damaged spinal cord (Faulkner & Keirstead, 2005; Keirstead *et al*, 2005; Sharp *et al*, 2010; All *et al*, 2012; Wang *et al*, 2013; Douvaras *et al*, 2014). However, the clinical application of pluripotent stem cell derivatives is limited due to the tumorigenic potential of the residual undifferentiated stem cells after transplantation (Miura *et al*, 2009; Fong *et al*, 2010). Direct lineage conversion of one somatic cell type into other cell types, such as myoblasts, neuronal cells, hepatocytes, cardiomyocytes, and endothelial cells, has been developed, which eliminates tumorigenicity through bypassing an intermediate pluripotent state (Davis *et al*, 1987; Efe *et al*, 2011; Huang *et al*, 2011, 2014; Sekiya & Suzuki, 2011; Li *et al*, 2013; Han *et al*, 2014; Morita *et al*, 2015). Meanwhile, this strategy is still challenging since the induced cells are in the postmitotic state, which impedes the large-scale expansion of desired cell types. Previous studies reported generation of expandable induced neural progenitor cells (iNPCs) from fibroblasts using distinct sets of neural transcription factors or reprogramming factors (Kim *et al*, 2011; Mitchell *et al*, 2014b). However, the low differentiation efficiency of iNPCs to mature oligodendrocytes limits its application as a SCI treatment. Thus, self-renewing and bipotent OPCs rather than iNPCs are considered as more appropriate cell source for developing cell-based therapies for SCI. Recently, two research

1 Hans Schöler Stem Cell Research Center (HSSCRC), School of Life Sciences, Ulsan National Institute of Science and Technology (UNIST), Ulsan, South Korea
2 Max Planck Partner Group-Molecular Biomedicine Laboratory (MPPG-MBL), UNIST, Ulsan, South Korea
3 Group of Computational Biology and Bioinformatics, Biodonostia Health Research Institute, San Sebastián, Spain
4 IKERBASQUE, Basque Foundation for Science, Bilbao, Spain
5 Department of Pediatrics and BK21 Project for Medical Sciences, Yonsei University College of Medicine, Seoul, South Korea
6 Department of Cell and Developmental Biology, Max Planck Institute for Molecular Biomedicine, Münster, Germany
*Corresponding author. Tel: +82 52 217 5201; Fax: +82 52 217 5269; E-mail: jbkim@unist.ac.kr

groups have reported generation of induced oligodendrocyte progenitor cells (iOPCs) from murine fibroblasts with combinations of transcription factors including *Sox10, Olig2,* and *Nkx6.2* (Najm *et al*, 2013) or *Sox10*, *Olig2*, and *Zfp536* (Yang *et al*, 2013). However, these cells can be expanded for only up to five passages and are restricted exclusively to the oligodendrocyte lineage (Najm *et al*, 2013). Moreover, the global gene expression profile of these iOPCs is distinct from the wild-type OPCs (wtOPCs) (Yang *et al*, 2013).

Our previous studies revealed that ectopic expression of *Oct4* alone can induce pluripotency in both mouse and human NSCs (Kim *et al*, 2009a,b,c). Remarkably, a number of recent studies showed Oct4-mediated direct reprogramming (Mitchell *et al*, 2014a) can promote direct lineage conversion of fibroblasts into blood progenitor cells (Szabo *et al*, 2010) as well as neural progenitor cells (Mitchell *et al*, 2014b), astrocytes into neural stem cells (Corti *et al*, 2012), or peripheral blood cell into neural progenitor cells (Lee *et al*, 2015) through passing cell plasticity stage (Mitchell *et al*, 2014a). Here, we demonstrated that the ectopic expression of *Oct4* with defined culture conditions is sufficient to generate homogeneous, self-renewing and bipotent iOPCs from fully differentiated somatic cells through passing the aggregate stage and demonstrates its functionality in rat SCI models. Our strategy reduces host genome modifications by minimizing the use of transcription factors to a single factor and facilitates future therapeutic applications for demyelinating conditions, including SCI.

Results

Generation of iOPCs from adult mouse fibroblasts by *Oct4*

To generate induced oligodendrocyte progenitor cells (iOPCs) using a minimal number of transcription factors, we employed Oct4-mediated direct reprogramming strategy, which induces cell fate plasticity at the early phase of reprogramming through mediating ectopic expression of *Oct4* (Mitchell *et al*, 2014a; Xu *et al*, 2015). The procedure for generating iOPCs is summarized in a schematic design (Stage 1; Fig 1A). Briefly, we first isolated the mouse skin fibroblasts from 6-week-old adult mice as parental cells and confirmed that the cells did not express pluripotency or neural-lineage markers (Fig EV1A–C). The fibroblasts were transduced with retroviruses encoding *Oct4* and cultured in defined OPC induction medium. The transduced cells underwent morphological changes into spindle-shaped cells 14–21 days after *Oct4* induction (Fig 1B and C), whereas uninfected cells did not change during the entire process (Fig 1D). Next, we mechanically isolated the cells exhibiting spindle-shaped morphology and replated them in OPC medium supplemented with platelet-derived growth factor AA (PDGF–AA), an essential mitogen for OPCs (Noble *et al*, 1988; Raff *et al*, 1988; Richardson *et al*, 1988; Hu *et al*, 2012). Within 35 days after infection, these cells formed floating OPC aggregates (OPC-AGs) (Stage 2; Fig 1E), and the OPC-AGs were subsequently transferred onto gelatin-coated plates in OPC medium. Bipolar OPC-like cells outgrew from the attached OPC-AGs and could be maintained in a highly homogeneous monolayer culture (Stage 3; Fig 1F and G). After consecutive passages, we established two iOPC clones named iOPC-C1 and iOPC-C2. Immunostaining revealed that the iOPC clones co-expressed OPC-specific surface markers, A2B5, PDGFRα, and NG2, and also expressed an early OPC marker, Olig2 (Fig 1H). We further evaluated whether iOPCs can maintain the proliferation after multiple passages. Both iOPC clones were stably expanded for more than 31 passages (Fig 1I). The mean population doubling times (mDT) of iOPC clones were approximately 26 h at both passages 3 (P3) and 31 (P31) (Fig 1J). We next confirmed the integration of *Oct4* transgene in the host genome of iOPC clones by genomic polymerase chain reaction (PCR) (Fig EV1D). Exogenous expression of *Oct4* mRNA was dramatically silenced in both clones at passage 5 (P5), as examined by quantitative reverse transcription–PCR (qRT–PCR) (Fig EV1E). Furthermore, the iOPCs maintained a normal mouse chromosome karyotype ($2n = 40$) after *Oct4* induction (Fig EV1F). These results support that *Oct4* expression with our defined culture condition is sufficient to convert the cell fate of adult mouse fibroblasts into expandable iOPCs.

Self-renewing iOPCs can differentiate into mature oligodendrocytes and astrocytes

Next, we investigated the self-renewal capacity and bipotency of iOPCs through examining populations of iOPCs, oligodendrocyte, astrocyte, and neurons at early (P5) and late passage (P35) in the OPC culture condition. Both iOPC clones homogeneously expressed A2B5, PDGFRα, and NG2. In contrast, glial fibrillary acidic protein $(GFAP)^+$ astrocytes were rarely present, and neither receptor-interacting protein $(RIP)^+$ mature oligodendrocytes nor neuron-specific class III beta-tubulin $(Tuj1)^+$ neurons were detected (Figs 2A and B, and EV2A). The mean percentage of positive cells for each marker is presented in Appendix Table S1. We next examined the bipotency of iOPCs to differentiate to both mature oligodendrocytes

Figure 1. Generation and characterization of *Oct4*-induced OPCs from fibroblasts.

A Experimental scheme for generating iOPCs from fibroblasts through Oct4-mediated reprogramming and *in vitro* differentiation into mature oligodendrocytes (OPC-AGs, OPC aggregates).

B–G Morphology of *Oct4*-infected fibroblasts in OPC induction medium (B) at 14 days post-infection. (C) Zoomed image of the white square in (B), which shows a spindle-shaped morphology. (D) Typical morphology of fibroblasts in OPC medium without *Oct4* induction. (E) Appearance of OPC-AGs within 35 days after infection. (F) OPC-like cells outgrew from OPC-AGs on gelatin-coated plates. (G) Zoomed image of the white square in (F), which shows the bipolar morphology of OPC-like cells. Scale bars, 250 μm.

H Immunofluorescence images of iOPC-C1 and iOPC-C2 stained with OPC-specific markers, A2B5, PDGFRα, NG2, and Olig2, in OPC medium. Cells were co-stained with A2B5 and PDGFRα (left-most columns), A2B5 and NG2 (left-middle columns), NG2 and PDGFRα (right-middle columns), and Olig2 and DAPI (right-most column). Cells were counterstained with DAPI. Scale bars, 75 μm.

I Morphology of iOPC clones at early (passage 3) and late passages (passage 31). Scale bars, 125 μm.

J Growth curves and mean doubling time (mDT) of iOPC clones at passage 3 (P3) and passage 31 (P31). Each point refers to the cell numbers of two iOPC clones every 24 h. Data are presented as the means ± SD ($n = 3$).

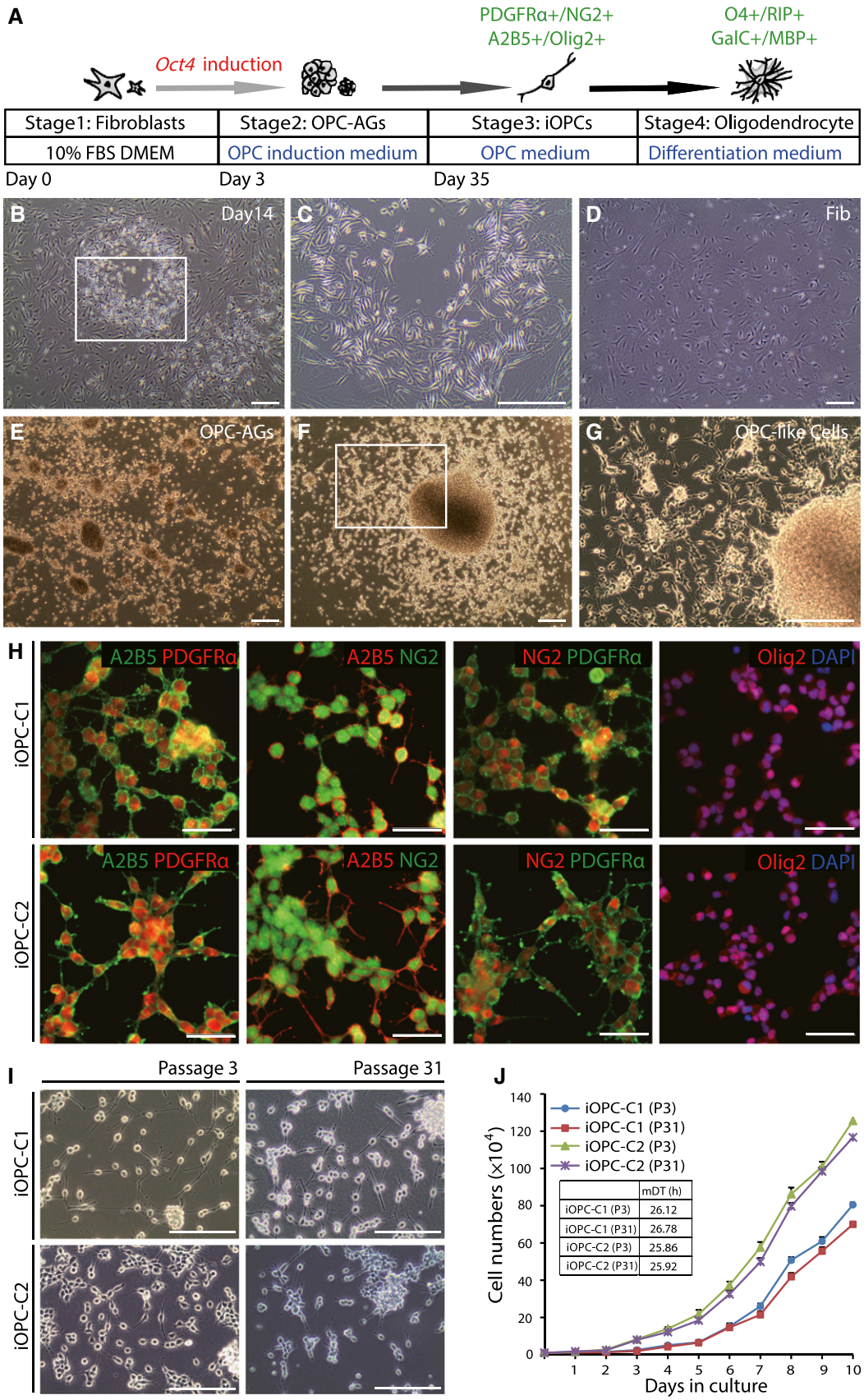

Figure 1.

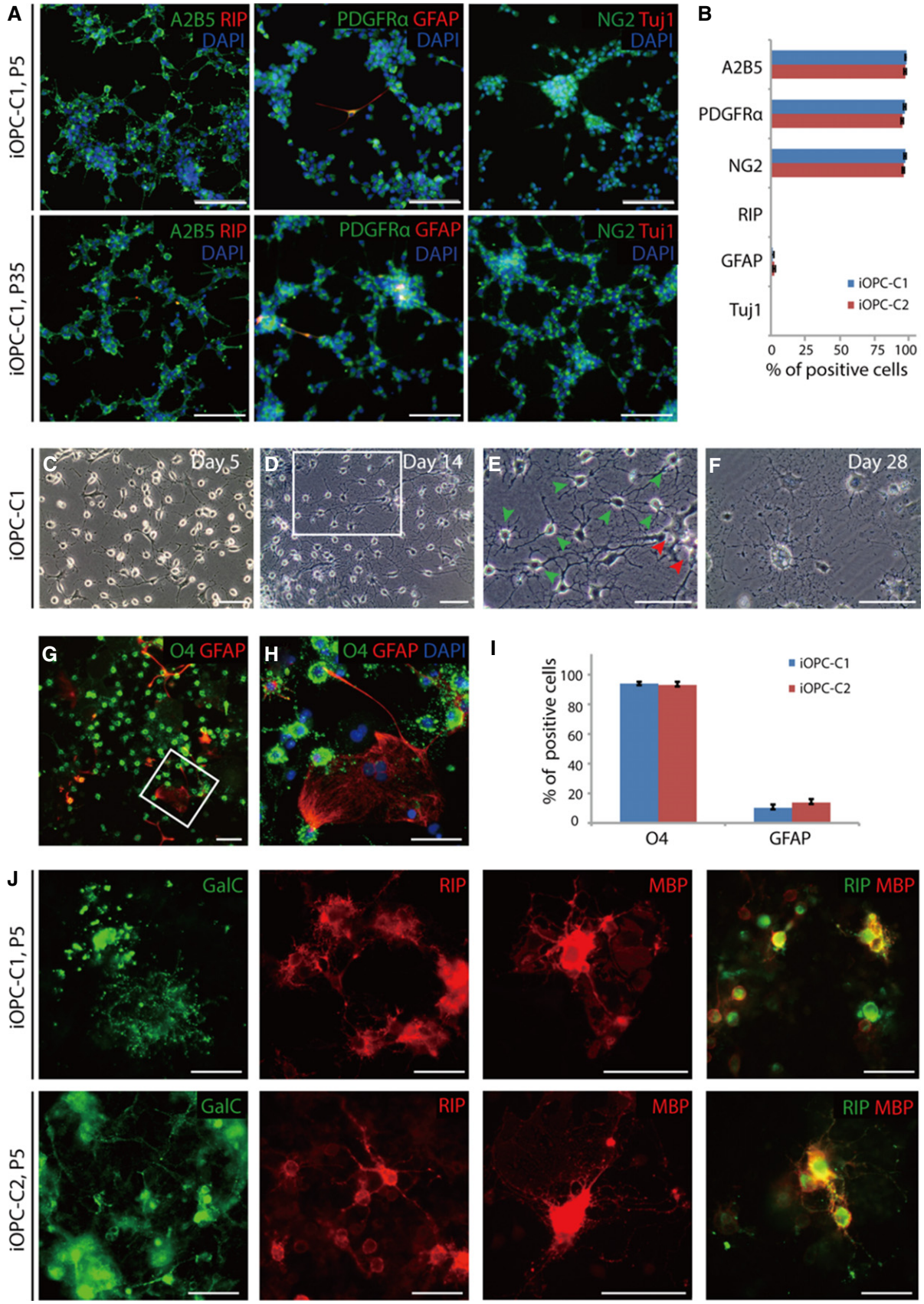

Figure 2.

Figure 2. Self-renewal capacity and biopotency of iOPCs.

A Immunofluorescence images of iOPC-C1 at passage 5 (P5) and 35 (P35) stained with A2B5 and RIP (left columns), PDGFRα and GFAP (middle columns), and NG2 and Tuj1 (right columns). Cells were counterstained with DAPI. Scale bars, 125 μm.

B Quantification of A2B5$^+$, PDGFRα$^+$, NG2$^+$, RIP$^+$, GFAP$^+$, and Tuj1$^+$ cells in undifferentiated iOPCs. Each type of marker-positive cells was counted in three biological replicates. Data are presented as the means ± SD (n = 3).

C–F Morphological changes of iOPC-C1 during differentiation on PDL/laminin-coated plates at (C) days 5, (D, E) 14, and (F) 28. (E) Zoomed image of the white square in (D) shows the mature oligodendrocytic morphology with complex branches (green arrowhead) and heterogeneous astrocytic morphology (red arrowhead). Scale bars, 50 μm.

G, H Biopotency of iOPC *in vitro* after 2 weeks of differentiation showing (G) O4-immunostained oligodendrocytes and GFAP-stained astrocytes derived from iOPC-C1. (H) Zoomed image of the white square in (G). Scale bars, 75 μm.

I The differentiation efficiency of iOPCs into O4$^+$ oligodendrocytes and GFAP$^+$ astrocytes. Data are presented as the means ± SD (n = 3).

J Expression of the premyelinating oligodendrocytes markers GalC (left-most columns), mature oligodendrocytes RIP (left–middle columns), and MBP (right–middle columns) and co-expression of RIP and MBP (right-most columns) at late stage of maturation of iOPC clones (P5). Scale bars, 75 μm.

and astrocytes. iOPCs at P5 were seeded onto PDL/laminin-coated plates in oligodendrocyte differentiation medium supplemented with thyroid hormone (T3) (Stage 4; Fig 1A). Cellular morphology was dramatically changed within 5 days (Figs 2C and EV2B), and oligodendrocytes with branched structures and star-shaped astrocytes were detected throughout 28 days of differentiation (Figs 2D–F and EV2C–E). Furthermore, immunostaining revealed the co-existence of O4$^+$ oligodendrocytes (~94 ± 1.3%) and GFAP$^+$ astrocytes (~16.2 ± 1.9%) after differentiation (Fig 2G–I), whereas none of the cells differentiated to neurons or oligodendrocytes in neuronal differentiation medium (Fig EV2F). These results indicate that iOPCs are glial lineage-restricted bipotent progenitors. Moreover, we observed differentiation of iOPCs to galactosylceramidase (GalC)$^+$ premyelinating oligodendrocytes, and RIP and myelin basic protein (MBP) co-expressing mature oligodendrocytes with complex branches in the late stage of maturation (Fig 2J). Remarkably, the iOPCs were able to differentiate to mature oligodendrocytes at late passage (P35) as well (Fig EV2G). The differentiation efficiency of iOPCs to each mature oligodendrocyte marker-positive cell along with GFAP$^+$ astrocyte is presented in Appendix Table S2. These results demonstrate that self-renewing and bipotent *Oct4*-iOPCs can differentiate to mature oligodendrocytes and astrocytes, but not to the neuronal lineage.

Oct4-iOPCs exhibit similar global gene expression profiles as wild-type OPCs

To investigate whether the iOPCs exhibit molecular similarity with wild-type OPCs (wtOPCs), we compared global gene expression patterns among fibroblasts (Fib), *Oct4*-infected cells at day 3 (FOct4-D3) and day 10 (FOct4-D10), mock-infected cells, iOPC clones at P5, and wtOPCs derived from pluripotent stem cells (Najm *et al*, 2013). Heat map analysis revealed that the global gene expression patterns of both iOPC clones were very similar to wtOPCs (Fig 3A), but distinct from the parental fibroblasts and the mock-infected cells. We analyzed the heat map further by selecting 80 genes that are commonly up-regulated in the iOPCs and wtOPC and classified them through Gene Ontology (GO) term enrichment profiling. We found most of the GO terms associated with the 80 genes are "oligodendrocyte/neural development" and "myelination" (Appendix Table S3). We narrowed down the 80 genes to 32 OPC and oligodendrocyte lineage-specific genes (Cahoy *et al*, 2008) and found high level of similarity in the expression levels of the 32 genes (Fig 3B). Moreover, pairwise scatter plots demonstrated high similarity between wtOPCs and iOPCs especially in OPC-specific genes, including *Mag, Nkx2.2, Olig1, Olig2, Sox10, Cnp*, *Cspg4,* and *Ptprz1,* distinct from the fibroblast (Fig 3C). The hierarchical clustering, 3D PCA analysis, and the distance map showed that iOPCs and wtOPCs are tightly correlated (Fig 3D and Appendix Fig S1A and B). To validate the microarray data, we examined the mRNA expression of OPC-specific genes including *Ptprz1, Siat8a, Nkx2.2, Olig1, Olig2, Sox10, Cnp, Mag,* and *Myrf* by qRT–PCR. Consistent with the microarray result, the expression level of OPC-specific genes was up-regulated in the iOPC clones relative to the fibroblasts (Fig 3E). Together, these results revealed a high degree of similarity in molecular identity between iOPCs and wtOPCs.

Oct4-iOPCs enhance recovery in a rodent spinal cord injury model

To examine the *in vivo* functionality of the iOPCs, we transplanted GFP-labeled iOPCs into adult rat SCI models (n = 8). We induced contusive damage to thoracic vertebrae 9 (T9) of the spinal cord and injected 1.2×10^5 iOPCs at P5 into the upper (T8) and lower (T10) vertebrate after 1 week of injury. To confirm the tissue recovery of the injury site, we conducted hematoxylin and eosin (H&E) staining of coronal and sagittal sections of the rat spinal cord after 6 weeks of transplantation. Transplanted iOPCs promoted the

Figure 3. Global gene expression profiles of *Oct4*-induced OPCs.

A, B Heat map analysis of (A) the global gene expression profiles and (B) 32 OPC and oligodendrocyte lineage enriched genes of Fib, FOct4-D3, FOct4-D10, mock, iOPC-C1, iOPC-C2, and wtOPCs. The upper color bar codifies the gene expression in the $\log_2$ scale. Shown are 767 probes selected based on codified variation ≥ ± 4 across all samples.

C Pairwise scatter plots of the global gene expression of wtOPCs versus iOPC-C1/iOPC-C2, iOPC-C1 versus iOPC-C2 and Fib versus iOPC-C1/iOPC-C2/wtOPC. The black lines indicate the boundaries of twofold changes in gene expression. The OPC-enriched genes (*Mag, Nkx2.2, Olig1, Olig2, Sox10, Cnp*, *Cspg4*, and *Ptprz1*) are highlighted with orange circles. Gene expression levels are shown on a $\log_2$ scale.

D Hierarchical clustering of wtOPCs, iOPC-C1, iOPC-C2, Fib, FOct4-D3, and FOct4-D10.

E qRT–PCR analysis of mRNA expression level for OPC lineage-specific genes (*Ptprz1, Siat8a, Nkx2.2, Olig1, Olig2, Sox10, Cnp, Mag*, and *Myrf)* in iOPCs relative to fibroblasts. Graphs represent $\log_2$-fold changes after normalization to *GAPDH*. Data are presented as the means ± SD (n = 3).

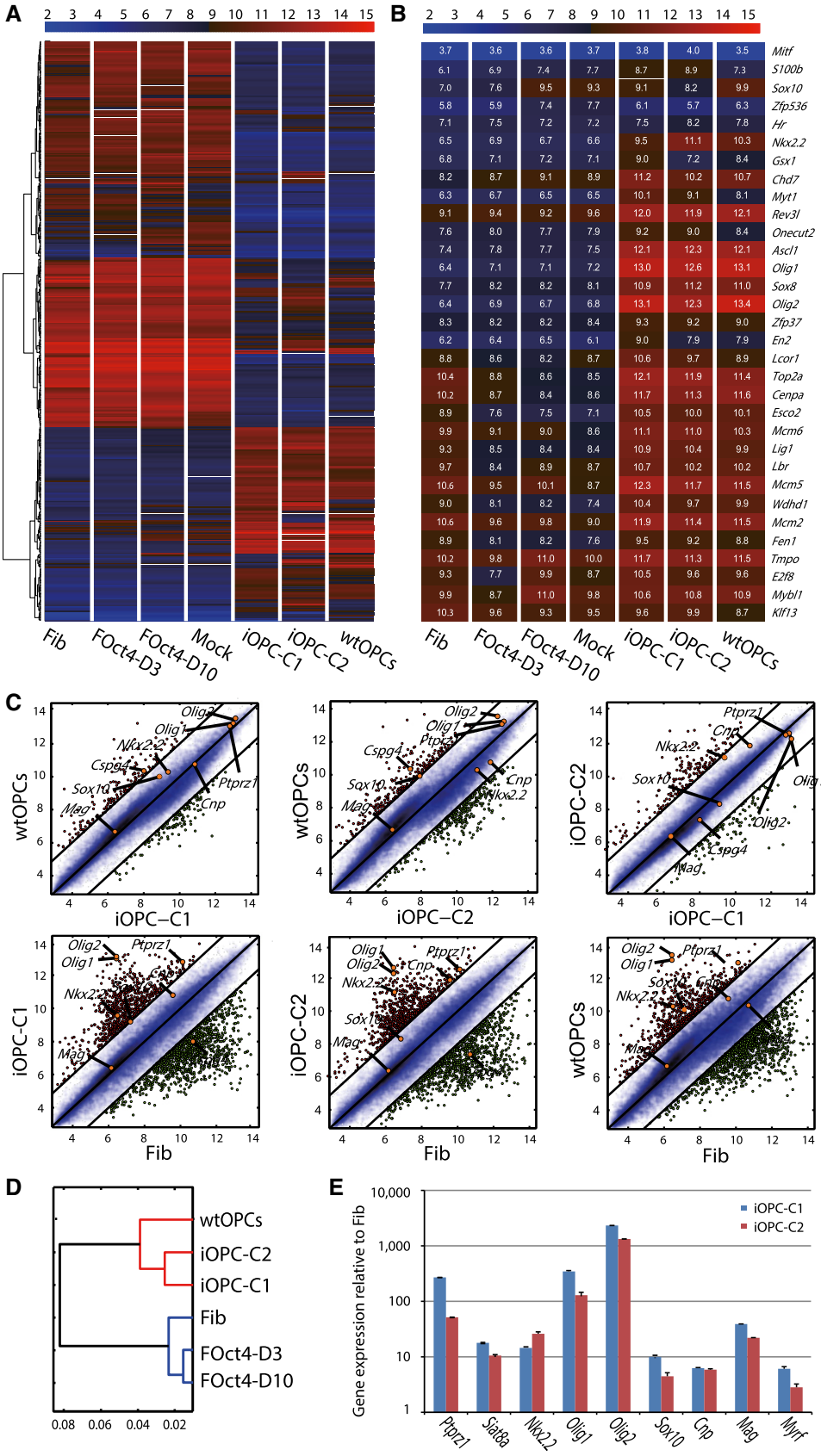

Figure 3.

recovery of spinal cord in the shape and reduced cavity size compared with vehicle-injected control (Fig 4A and B). Furthermore, we observed robust engraftment of the transplanted GFP^+ iOPCs that migrated toward the injury site (Fig 4C and D). Next, we immunostained tissue slides with MBP to investigate whether engrafted iOPCs contribute to myelination *in vivo* (Fig 4E and F). GFP^+ iOPCs were distributed in the vicinity of the myelinated nerve fibers in the white matter (Fig 4G and H). This result suggests that myelination was associated with the transplanted iOPCs. To identify the cellular features of iOPCs in the SCI model, we assessed *in vivo* differentiation potential of the iOPCs. Most of the GFP^+-engrafted cells robustly expressed mature oligodendrocyte markers such as CNPase, MBP, APC-CC1, and O4 (Figs 4I and J, and EV3A and B) and were mainly localized near neurofilament $(NF)^+$ host neurons in the injury site (Figs 4K–N and EV3C and D). The interaction between iOPC-derived mature oligodendrocyte ($GFP^+CNPase^+$/GFP^+MBP^+/$GFP^+AP\text{-}CC1^+$) and the host NF^+ neurons in the injury site was clearly observed in the three-dimensional reconstructed images (Figs 4O and P and EV3E, and Movie EV1). These results strongly indicate differentiation of the transplanted iOPCs into myelin-producing oligodendrocytes that enhance the remyelination process by ensheathing damaged neurons. In addition, a few astrocytes (GFP^+GFAP^+) (Fig EV3F–H) and undifferentiated iOPCs ($GFP^+PDGFR\alpha^+$/GFP^+A2B5^+/GFP^+NG2^+/GFP^+Olig2^+) were observed as well (Fig EV3I). We further examined *in vivo* differentiation potential of iOPCs in mouse SCI models ($n = 4$) and observed expression of A2B5, PDGFRα, CNPase, and GFAP from the engrafted cells in the mouse spinal cord tissue as well (Fig EV3J–Q). Next, we evaluated the motor function recovery of the hind limbs by measuring Basso–Beattie–Bresnahan (BBB) scores for 10 weeks in rat SCI models that were treated either with PBS (control) ($n = 10$) or with iOPCs injection ($n = 8$). Both groups exhibited regaining motor ability for the first 2 weeks of the injury due to the natural reflex recovering ability in rats (Basso *et al*, 1995). However, rats transplanted with iOPCs improved in BBB scores from week 2 ($n = 8$) that persisted steadily through week 10 ($n = 4$) showing significant improvement in locomotor recovery ($P < 0.05$), which is distinct from the control group which reached the plateau in the BBB score by week 2 (Fig 4Q). To assess the risk of tumor formation, we subcutaneously transplanted iOPCs (P5) into severe combined immunodeficient (SCID) mice and no tumors were observed for 9 months of experiment period (Fig EV3R). These results show that iOPCs can differentiate into mature oligodendrocytes and astrocytes without tumor formation *in vivo* and successfully promote functional recovery of locomotion in a SCI model.

Discussion

Here, we have successfully generated self-renewing iOPCs from adult mouse fibroblasts through Oct4-mediated direct reprogramming methodology. Conventionally, OPCs were isolated from fetal brain or derived from pluripotent stem cells (Sim *et al*, 2011; All *et al*, 2012; Wang *et al*, 2013). However, primary OPCs are limited in availability, and pluripotent stem cell-derived OPCs have the risk of tumor formation after transplantation and are low in differentiation efficiency. In contrast, the direct lineage conversion strategy has the advantage in high-yield generation of the desired cells without the tumorigenic potential by bypassing an intermediate pluripotent state (Najm *et al*, 2013; Yang *et al*, 2013). Recent studies revealed that iOPCs can be generated from mouse and rat fibroblasts by defined sets of lineage-specific transcription factors, including *Sox10*, *Olig2*, and *Nkx6.2* (Najm *et al*, 2013) or *Sox10*, *Olig2*, and *Zfp536* (Yang *et al*, 2013). However, the iOPCs generated by *Sox10*, *Olig2*, and *Nkx6.2* transgenes were not bipotent OPCs as they cannot be differentiated into astrocytes, and they were expandable up to only 5 passages (Najm *et al*, 2013). In addition, the global gene expression pattern of the iOPCs generated by *Sox10, Olig2,* and *Zfp536* transgenes exhibited a transcription profile that is more similar to primary pre-oligodendrocytes than the OPCs (Yang *et al*, 2013).

In contrast to the previously reported direct conversion methods for generating iOPCs, we showed that a single transcription factor *Oct4* in combination with defined OPC induction medium is sufficient to generate iOPCs from the mouse fibroblast. Previous studies reported that fewer viral integrations were detected in single-factor-derived iPSCs (Kim *et al*, 2009b) compared with iPSCs generated by four transcription factors, thereby reducing chances of insertional mutagenesis (Wernig *et al*, 2007; Aoi *et al*, 2008). Thus, our single-factor-derived iOPCs would have higher levels of genomic stability by having lower chance of viral integration into the host genome than the previously reported three-factor-derived iOPCs. Moreover, the previous studies isolated iOPCs by purifying proteolipid protein $(Plp)^+$ or $O4^+$ cells from a heterogeneous population (Najm *et al*,

Figure 4. Therapeutic potential and differentiation capacity of transplanted iOPCs in a spinal cord injury model.

A, B H&E staining of rat spinal cords at 6 weeks after transplantation with (A) vehicle or (B) iOPC-C1 (left, coronal plane section; right, sagittal plane section). Black arrowheads indicate the injury sites (a' and b') of each group. Scale bars, 400 μm.

C, D Immunofluorescence image of (C) GFP-labeled iOPC-C1 in a sagittal section of the rat spinal cord. (D) Zoomed image of the yellow square in (C) showing the migration of transplanted cells toward the injury site. Scale bars, 500 μm.

E–H Immunohistochemical analysis of the white matter of the rat spinal cord transplanted with iOPCs (E) for MBP revealing localization of GFP^+ iOPC-derived oligodendrocytes at myelinated nerve fiber structures. Staining was visualized by diaminobenzidine (DAB). Zoomed image of the black square in (E) shows (F) DAB-stained MBP, (G) locality of GFP^+ oligodendrocytes, and (H) co-localization of GFP^+ oligodendrocytes and MBP. Scale bars, 150 μm.

I–P Expression of the mature oligodendrocyte markers (I) CNPase and (J) MBP in transplanted GFP^+ iOPC-C1. Cells co-expressing GFP and oligodendrocyte markers are indicated with white arrowheads. (K, L) GFP^+ cells (white arrowheads) wrap neurofilaments (NF) stained host neurons. Confocal *z*-stacks of the indicated area (asterisks) show that NF^+ host neurons are surrounded by (M) $GFP^+CNPase^+$ or (N) GFP^+MBP^+ cells. (O, P) Three-dimensional reconstructions of rat spinal cord sections using IMARIS software show the complex structure of the host neurons and GFP^+ cells forming axon ensheathments. Co-expression (yellow) of GFP^+ iOPCs (green) and mature oligodendrocyte markers (red) is observed around neurons (blue). Scale bars, 30 μm.

Q BBB score evaluation of the left (left panel), right (middle panel), and average (right panel) of both hind limbs during the 10 weeks following transplantation. Data are presented as the means ± SD ($n = 3$–8). *$P < 0.05$ (one-way ANOVA).

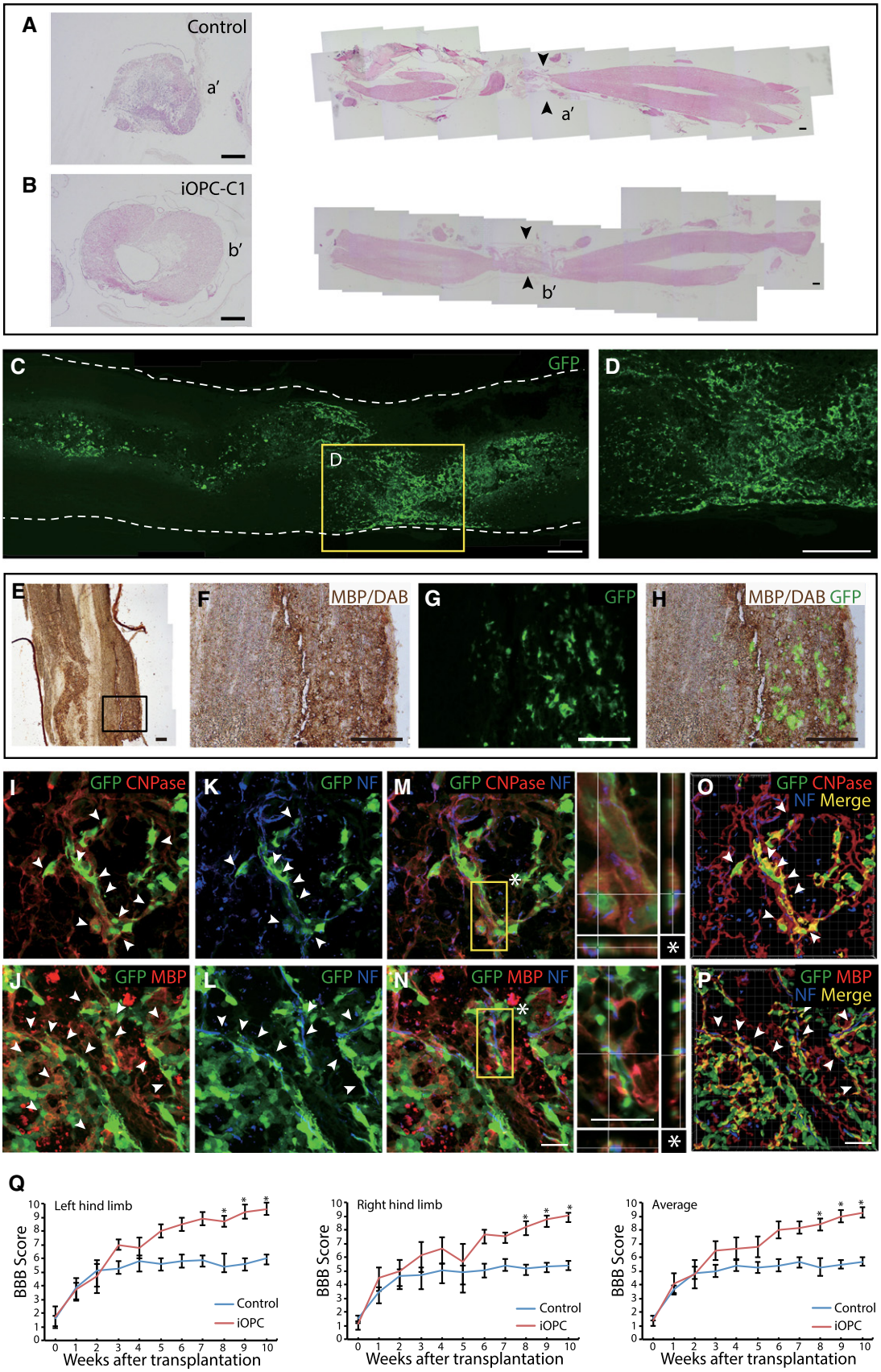

Figure 4.

2013; Yang *et al*, 2013). However, the iOPCs in these studies may include heterogeneous population having various viral integration sites in the host genome. Moreover, Plp and O4 are also expressed in pre-oligoendrocytes as well as mature oligodendrocytes which interrupt isolation of homogeneous OPC population. Therefore, the purifying method used in the previous studies yields difficulty in developing a single homogeneous cell line, which leads to the difficulty in determining the accurate conversion efficiency. In contrast, we demonstrated a clonal reprogramming method, as we have shown previously in generation of iPSCs from NSCs (Kim *et al*, 2009c). This approach enables the establishment of homogeneous cell lines from single colonies. Additionally, as the previous direct conversion strategies have demonstrated low conversion efficiencies, it is not feasible to obtain iOPCs with high yield and purity. Our iOPCs are self-renewing and bipotent progenitors that maintain typical OPC features including bipolar morphology, OPC marker expression, and high differentiation efficiency *in vitro* and *in vivo* throughout multiple passages (> 31 passages). Strikingly, the global gene expression pattern of *Oct4*-iOPCs exhibits high levels of similarity to the publically available GEO data sets of wtOPCs (Najm *et al*, 2013). Lastly, we generated iOPCs through sequential induction with defined medium at each stage to induce the target cell fate more precisely. Thus, our strategy allows generation of a pure population of proliferative iOPCs that resembles key morphological and molecular features of wtOPCs in large scale.

Recent studies demonstrated that transplantation of OPCs differentiated from ESCs or iPSCs is a promising strategy to promote recovery after SCI (Keirstead *et al*, 2005; Sharp *et al*, 2010; Czepiel *et al*, 2015). However, the risk of tumorigenicity from undifferentiated cells remains as a major challenge for its therapeutic use. In this study, *Oct4*-iOPCs differentiated to mature oligodendrocytes and surrounded host neurons, displaying extensive ensheathment when transplanted into the rodent SCI model. Notably, the transplantation of iOPCs facilitated remyelination and significant locomotor functional recovery without tumor formation. Thus, *Oct4*-iOPCs can serve as a prospective cell source for the establishment of cell-based therapy for SCI. To note, we mainly focused on a rat SCI model because of the small size of the mouse SCI models that limits surgical maneuvers and device implantations (Nakae *et al*, 2011). However, rat models are commonly used interchangeably with mouse models due to its cost and convenience in surgical maneuvers (Talac *et al*, 2004).

Several lines of evidence have demonstrated that *Oct4* is involved in the initial cell fate commitment during reprogramming. Previously, we reported that *Oct4* is required to induce NSCs towards the pluripotent state, which validates the critical role of *Oct4* in cell fate determination (Kim *et al*, 2008; Kim *et al*, 2009a,b,c). Here, we generated iOPCs by using a similar approach to the recent works on generation of iNPCs or blood progenitors from somatic cells through OCT4-mediated direct reprogramming (Szabo *et al*, 2010; Mitchell *et al*, 2014b; Lee *et al*, 2015). The previous studies signify the importance of the lineage-specific induction medium since *Oct4*-induced somatic cell fate determination seems to depend on the lineage-specific culture condition (Szabo *et al*, 2010; Mitchell *et al*, 2014a,b; Lee *et al*, 2015). Specifically, the recent work on blood-derived hiNPCs showed that blood cells can be directly reprogrammed into iNPCs by using *OCT4* in combination with bFGF and epidermal growth factor (EGF)-supplemented NPC induction medium, and small molecules (SMAD and GSK-3 inhibitors) (Lee *et al*, 2015). In the same line, we used OPC induction medium supplemented with PDGF-AA, an essential OPC-inducing growth factor (Hu *et al*, 2012), to convert the cell fate of *Oct4*-induced fibroblast into iOPC. Therefore, our study demonstrated *Oct4*-induced somatic cell fate can be determined to OPC lineage by providing OPC lineage-specific culture condition. Importantly, we did not obtain any $Tuj1^+$ neurons in the process of generating iOPCs (Figs 2A and EV3A) and from the iOPCs under neuronal induction condition (Fig EV3F). Thus, these results suggest that transient NPC state was not involved during the reprogramming, possibly due to the OPC lineage-specific stimuli in our OPC induction medium. However, a detailed signaling pathway that mediates generation of iOPCs through bypassing NPC state remains to be elucidated.

In conclusion, we demonstrated that *Oct4* with defined iOPCs induction condition reprograms adult somatic cells into self-renewing and bipotent iOPCs, thereby allowing large-scale expansion of the oligodendrocytes and astrocytes. This single-factor-mediated conversion method is a safer and simpler protocol that potentially reduces the chance of viral insertional mutagenesis. Although further investigation is needed to study the mechanism of *Oct4*-triggered lineage conversion, our strategy may provide the basis for future human iOPC generation and new insights to investigate high-throughput drug screening and stem cell-based therapies for SCI and demyelinating disorders.

Materials and Methods

Isolation of mouse skin fibroblasts

The experimental procedures were approved by the Animal Care and Use Committee at Ulsan National Institute of Science and Technology (Ulsan, South Korea). Primary dermal fibroblasts were isolated from skin biopsies of 6-week-old CF1 mice (Jackson Laboratories) as described previously (Driskell *et al*, 2013) and cultivated in fibroblast medium [DMEM high glucose (GIBCO), 10% fetal bovine serum (GIBCO), penicillin/streptomycin (GIBCO), non-essential amino acids (GIBCO), and β-mercaptoethanol (GIBCO)] MEF medium. Parental fibroblasts were passaged 2–3 times before *Oct4* induction.

Virus production

To produce viruses, a pMX-based retroviral vector containing *Oct4* cDNA (Addgene #13366) and the SFFV–GFP lentiviral vector, a gift from Dr. Axel Schambach (Warlich *et al,* 2011), were transfected into 293T cells using the X-tremeGENE9 DNA transfection reagent (Roche) to package the VSV-G-pseudotyped virus. After 48 h of transfection, the virus-containing supernatants were collected and filtered through a 0.45-μm syringe filter. The viruses were harvested as previously described (Zaehres & Daley, 2006).

Generation of iOPCs

Primary adult mouse fibroblasts were seeded at 1×10^4 cells on gelatin-coated 6-well plates. On the next day, the fibroblasts were infected with a pMX retroviral vector expressing *Oct4* in

MEF medium containing 6 μg/ml protamine sulfate. The viral supernatant was removed after 24 h of infection and replaced with fresh MEF medium. At 3 days post-infection, the medium was switched to OPC induction medium (1:1 mixture of DMEM/F12 (GIBCO) and neurobasal medium (GIBCO) supplemented with N2 (GIBCO), B27 (GIBCO), penicillin/streptomycin, 10 ng/ml PDGF-AA (Peprotech), and 10 ng/ml FGF2 (Peprotech)). *Oct4*-infected cells were mechanically isolated by a glass micropipette and transferred into defined OPC medium (DMEM/F12 supplemented with N2, penicillin/streptomycin, 20 ng/ml PDGF-AA (Peprotech), and 10 ng/ml FGF2). The floating aggregates were re-plated onto gelatin-coated plate, and the OPC-like cells were subsequently passaged 3–5 times until the cells become homogeneous. We conducted further characterization of the iOPCs at early passages (P3 and P5) and late passages (P31 and P35).

Oct4 transgene silencing analysis

Total RNA of iOPC-C1 and iOPC-C2 was extracted using an RNeasy mini kit (Qiagen). cDNAs were synthesized by SuperScript® III reverse transcriptase (Invitrogen), and 500 ng total RNA was obtained per reaction. Real-time PCR analysis was performed on a LightCycler 480 and SYBR Green I Master mix (Roche) in a total volume of 20 μl. The experiments were performed in triplicate, and expression was normalized to *GAPDH*. Gene expression was measured by the C_t calculation method. The sequences of the primers used in this experiment are listed in Appendix Table S5.

RT–PCR and quantitative RT–PCR

DNA-free total RNA of iOPC-C1 and iOPC-C2 (P5) was extracted using the RNeasy mini kit (Qiagen). Total RNA (500 ng) was used to synthesize cDNAs using SuperScript® III reverse transcriptase (Invitrogen). RT–PCR was performed using recombinant Taq DNA polymerase (Invitrogen). qRT–PCR analysis was conducted on a LightCycler 480 instrument with SYBR Green I Master mix (Roche). The experiments were performed in triplicate, and expression was normalized to the housekeeping gene *GAPDH*. Gene expression was measured by calculating C_t values. All of the experiments were conducted according to the manufacturer's instructions. The sequences of the primers used are listed in Appendix Table S5.

In vitro differentiation of iOPCs

1×10^4 iOPCs (P5 and P35) were seeded on PDL/laminin-coated 4-well plates in OPC medium. For oligodendrocyte differentiation, the medium was switched to oligodendrocyte differentiation medium 1, which contains DMEM/F12 supplemented with N2, penicillin/streptomycin, 10 ng/ml FGF2 (Peprotech), and 10 mM forskolin (Sigma-Aldrich), for 4–5 days. For further maturation, the medium was changed to oligodendrocyte differentiation medium 2, which contains 30 ng/ml 3,3′,5-triiodothyronine (T3; Sigma-Aldrich) and 20 ng/ml ascorbic acid (AA; Sigma-Aldrich). For astrocyte differentiation, we differentiated iOPCs in DMEM containing 2% FBS for 7–9 days. For neuronal differentiation, the cells were cultured in neuronal differentiation medium 1 (DMEM/F12 supplemented with N2, B27, and 10 ng/ml FGF-2) for 5 days and then switched to neuronal differentiation medium 2 (DMEM/F12: neurobasal (1:1) supplemented with 0.5% N2 and 0.5% B27) (Kim *et al*, 2009b).

Immunocytochemistry (ICC) analysis

iOPCs or iOPC derivatives were fixed with 4% paraformaldehyde for 10 min and permeabilized with 0.1% Triton X-100 for 10 min. The cells were then incubated in 4% FBS blocking solution for 30 min and subsequently incubated in primary antibodies diluted in blocking solution for 1 h at room temperature. After the primary antibody incubation, cells were washed with PBST (0.05% Tween-20) three times. The secondary antibodies were diluted in PBS and applied for 1 h: Alexa Fluor 488/568 anti-mouse IgG1, IgG3, IgM, and anti-goat IgG (Invitrogen, 1:1,000). Nuclei were stained with DAPI (Invitrogen). The primary antibodies used for ICC analysis are listed in Appendix Table S4.

Microarray analysis

Global gene expression of the following cell populations were profiled by microarray analysis: fibroblasts, FOct4-D3 (3 days after *Oct4* induction), FOct4-D10 (10 days after *Oct4* induction cultured in OPC medium), mock (mock-infected fibroblasts cultured in OPC medium for 10 days), iOPC-C1, and iOPC-C2. We compared these samples with previously published data for wtOPCs (undifferentiated OPCs from pluripotent stem cells) (Yang *et al*, 2013). Total RNA of iOPC clones (P5) was isolated using an RNeasy mini kit (Qiagen) according to the manufacturer's instructions. The samples were hybridized to an Affymetrix Mouse Gene 1.0 ST array. Normalization was performed with the robust multi-array analysis (RMA) algorithm (Irizarry *et al*, 2003). Data processing and graphic production were performed with in-house-developed functions in MATLAB. The hierarchical clustering of genes and samples was performed with the one minus correlation metric and the unweighted average distance (UPGMA) linkage method. Differentially expressed genes were analyzed by comparing gene expression of iOPC clones (iOPC-C1, iOPC-C2) relative to fibroblasts. Among the highly up-regulated genes (> 1.2-fold), genes that are related to neural/oligodendrocyte/OPC development or myelin function were screened according to Gene Ontology (GO) term enrichment profiling. Microarray data from the wtOPCs were downloaded from the GEO database (data accessible at NCBI GEO database (Najm *et al*, 2013), accession GSE45440). The data discussed in this publication were deposited in NCBI Gene Expression Omnibus (Edgar *et al*, 2002) and are accessible through GEO Series accession number GSE52035.

Contusion spinal cord injury and transplantation

The procedures were approved by the Animal Care and Use Committees of Yonsei University College of Medicine (Seoul, Korea). Adult male Sprague Dawley rats (220–240 g) and 6-week-old male severe combined immunodeficient (SCID) mice were anesthetized with intraperitoneal injections of ketamine (90 mg/kg), rompun (0.2 ml/kg), and promazine (1 mg/kg). The skin was shaved and decontaminated with serial 70% ethanol and povidone–iodine washes. A dorsal laminectomy was performed on the T9 vertebrae to expose the spinal cord. The contusion injury was induced at spinal segment T9 using the Infinite Horizon Impactor (Precision Systems,

Kentucky, IL, USA) with a force of 230 Kdyn. After contusion, the muscle and skin were sutured. For transplantation, iOPC-C1 (P5) was labeled with GFP by the lentiviral system, and the integrated cells were detected by green fluorescence. After 1 week of injury, 1.2×10^5 iOPCs were injected into T8 and T10 using a glass micropipette. The animals were provided food and water regularly and received manual bladder expression twice daily for urination.

Basso-Beattie-Bresnahan (BBB) test

The locomotor recovery of the animals was assessed by two independent observers using the BBB open-field locomotor score. The experiment was performed by blinded observation. The rat SCI models were separated into PBS-injected control group ($n = 10$) and 1.2×10^5 iOPCs (P5)-injected experimental group ($n = 8$) and were tested weekly for up to 10 weeks after transplantation. Hind limb locomotion was assessed by the BBB open-field scale as described previously (Basso *et al*, 1995).

Histological process and immunohistochemical (IHC) analysis

The rats were anesthetized and perfused in PBS at 6 weeks after transplantation. The spinal cords were fixed overnight in 4% paraformaldehyde and dehydrated using a series of alcohol and xylene. The tissue was embedded in paraffin blocks and sectioned sequentially at 16 μm in the sagittal or coronal planes. The sections were permeabilized with 0.2% Triton X-100 and blocked with CAS-Block solution (Invitrogen) to prevent non-specific binding. For IHC analysis, the sections were incubated with primary antibodies diluted in CAS-Block solution overnight at 4°C. After the primary antibody incubation, the cells were washed with PBST (0.05% Tween-20) three times for 10 min each. The following secondary antibodies were diluted in PBS and applied for 1 h: Alexa Fluor 405/488/568 anti-mouse IgG1, IgG3, IgM, anti-goat IgG, and anti-rat IgG (Invitrogen, 1:200). Fluorescence images were visualized with Olympus IX81-ZDC and FV1000 microscopes. The primary antibodies used for IHC analysis are listed in Appendix Table S4.

For diaminobenzidine (DAB) immunostaining, the tissue sections were incubated in the primary antibody and then treated with 0.3% H_2O_2 in PBS for 30 min at room temperature to block endogenous peroxidases. The sections were then incubated with a horseradish peroxidase-conjugated anti-rat IgG antibody (Invitrogen, 1:200) for 2 h. We used DAB (Invitrogen) to visualize the sections by treating them for 5 min at room temperature.

For hematoxylin and eosin staining, paraffin blocks were prepared by aforementioned method with SCI rats 6 weeks after transplantation. The paraffin blocks were sectioned sequentially at 4 μm in the sagittal or coronal planes. Nucleus was stained with hematoxylin (Sigma-Aldrich) and blued in 0.2% ammonium hydroxide. Tissue were then placed in Eosin Y solution (Sigma-Aldrich) and followed by several washings and dehydrating. Slides were mounted with mounting solution (Leica).

Karyotyping

The fibroblasts and iOPCs were treated with 0.1 μg/ml demecolcine (Sigma-Aldrich) for 8 h in a 37°C CO_2 incubator. The cells were collected and trypsinized into a single-cell suspension and then incubated in 75 mM KCl for 20 min at 37°C. Carnoy's solution (methanol:acetic acid = 1:3) was slowly added to the cells, which were then fixed for 5 min at room temperature. The cells were fixed twice more with fresh Carnoy's solution for 20 min each and dropped onto humid glass slides. The chromosomes clearly spread and were counted in individual cells.

Growth curve and mean doubling time

iOPC clones (1×10^4 cells) at P3 and P31 were seeded onto 4-well plates and cultivated for 10 days. The cells were collected from triplicate wells and manually counted each day (24 h) using a hemacytometer (Marienfeld). The average cell numbers on each day were plotted, and the mean doubling time was calculated based on the growth curve.

Data deposition

The microarray data reported in this article have been deposited in the NCBI Gene Expression Omnibus database under accession number GSE52035.

Statistical analysis

All data in this article are presented as the means ± SD (standard deviation). Data from at least three independent samples were used for statistical analysis. A P-value < 0.05 (one-way ANOVA) was considered significant.

Expanded View for this article is available online:
http://emboj.embopress.org

Acknowledgements
We thank Dr. Axel Schambach for providing SFFV-GFP, JY and SW for generous assistance in preparation of the manuscript. This research was partly supported by the Bio & Medical Technology Development Program of the National Research Foundation (NRF) and funded by the Ministry of Science, ICT & Future Planning [2012M3A9C6049788], the ICT R&D Program of MSIP/IITP [R0190-15-2072], and Max Planck Partner Group, Max Planck Society (MPG), Germany.

Author contributions
JBK designed and supervised the study. JBK and HL conducted most of the experiments and wrote the manuscript. MJA contributed to the microarray analysis. KIP and KH contributed to the animal experiments. DN and MRP collected the data and DN, MRP, HZ, and S-JL were involved in preparing the manuscript.

Conflict of interest
The authors declare that they have no conflict of interest.

References

All AH, Bazley FA, Gupta S, Pashai N, Hu C, Pourmorteza A, Kerr C (2012) Human embryonic stem cell-derived oligodendrocyte progenitors aid in functional recovery of sensory pathways following contusive spinal cord injury. *PLoS ONE* 7: e47645

Aoi T, Yae K, Nakagawa M, Ichisaka T, Okita K, Takahashi K, Chiba T, Yamanaka S (2008) Generation of pluripotent stem cells from adult mouse liver and stomach cells. *Science* 321: 699 – 702

Basso DM, Beattie MS, Bresnahan JC (1995) A sensitive and reliable locomotor rating scale for open field testing in rats. *J Neurotrauma* 12: 1 – 21

Ben-Hur T, Goldman SA (2008) Prospects of cell therapy for disorders of myelin. *Ann N Y Acad Sci* 1142: 218 – 249

Cahoy JD, Emery B, Kaushal A, Foo LC, Zamanian JL, Christopherson KS, Xing Y, Lubischer JL, Krieg PA, Krupenko SA, Thompson WJ, Barres BA (2008) A transcriptome database for astrocytes, neurons, and oligodendrocytes: a new resource for understanding brain development and function. *J Neurosci* 28: 264 – 278

Corti S, Nizzardo M, Simone C, Falcone M, Donadoni C, Salani S, Rizzo F, Nardini M, Riboldi G, Magri F, Zanetta C, Faravelli I, Bresolin N, Comi GP (2012) Direct reprogramming of human astrocytes into neural stem cells and neurons. *Exp Cell Res* 318: 1528 – 1541

Czepiel M, Boddeke E, Copray S (2015) Human oligodendrocytes in remyelination research. *Glia* 63: 513 – 530

Davis RL, Weintraub H, Lassar AB (1987) Expression of a single transfected cDNA converts fibroblasts to myoblasts. *Cell* 51: 987 – 1000

Douvaras P, Wang J, Zimmer M, Hanchuk S, O'Bara Melanie A, Sadiq S, Sim Fraser J, Goldman J, Fossati V (2014) Efficient generation of myelinating oligodendrocytes from primary progressive multiple sclerosis patients by induced pluripotent stem cells. *Stem Cell Rep* 3: 250 – 259

Driskell RR, Lichtenberger BM, Hoste E, Kretzschmar K, Simons BD, Charalambous M, Ferron SR, Herault Y, Pavlovic G, Ferguson-Smith AC, Watt FM (2013) Distinct fibroblast lineages determine dermal architecture in skin development and repair. *Nature* 504: 277 – 281

Edgar R, Domrachev M, Lash AE (2002) Gene Expression Omnibus: NCBI gene expression and hybridization array data repository. *Nucleic Acids Res* 30: 207 – 210

Efe JA, Hilcove S, Kim J, Zhou H, Ouyang K, Wang G, Chen J, Ding S (2011) Conversion of mouse fibroblasts into cardiomyocytes using a direct reprogramming strategy. *Nat Cell Biol* 13: 215 – 222

Faulkner J, Keirstead HS (2005) Human embryonic stem cell-derived oligodendrocyte progenitors for the treatment of spinal cord injury. *Transpl Immunol* 15: 131 – 142

Fong CY, Gauthaman K, Bongso A (2010) Teratomas from pluripotent stem cells: a clinical hurdle. *J Cell Biochem* 111: 769 – 781

Franklin RJM, Ffrench-Constant C (2008) Remyelination in the CNS: from biology to therapy. *Nat Rev Neurosci* 9: 839 – 855

Han JK, Chang SH, Cho HJ, Choi SB, Ahn HS, Lee J, Jeong H, Youn SW, Lee HJ, Kwon YW, Cho HJ, Oh BH, Oettgen P, Park YB, Kim HS (2014) Direct conversion of adult skin fibroblasts to endothelial cells by defined factors. *Circulation* 130: 1168 – 1178

Hu JG, Wang YX, Wang HJ, Bao MS, Wang ZH, Ge X, Wang FC, Zhou JS, Lu HZ (2012) PDGF-AA mediates B104CM-induced oligodendrocyte precursor cell differentiation of embryonic neural stem cells through Erk, PI3K, and p38 signaling. *J Mol Neurosci* 46: 644 – 653

Huang P, He Z, Ji S, Sun H, Xiang D, Liu C, Hu Y, Wang X, Hui L (2011) Induction of functional hepatocyte-like cells from mouse fibroblasts by defined factors. *Nature* 475: 386 – 389

Huang P, Zhang L, Gao Y, He Z, Yao D, Wu Z, Cen J, Chen X, Liu C, Hu Y, Lai D, Hu Z, Chen L, Zhang Y, Cheng X, Ma X, Pan G, Wang X, Hui L (2014) Direct reprogramming of human fibroblasts to functional and expandable hepatocytes. *Cell Stem Cell* 14: 370 – 384

Irizarry RA, Bolstad BM, Collin F, Cope LM, Hobbs B, Speed TP (2003) Summaries of Affymetrix GeneChip probe level data. *Nucleic Acids Res* 31: e15

Jin K, Xie L, Mao X, Greenberg MB, Moore A, Peng B, Greenberg RB, Greenberg DA (2011) Effect of human neural precursor cell transplantation on endogenous neurogenesis after focal cerebral ischemia in the rat. *Brain Res* 1374: 56 – 62

Keirstead HS, Nistor G, Bernal G, Totoiu M, Cloutier F, Sharp K, Steward O (2005) Human embryonic stem cell-derived oligodendrocyte progenitor cell transplants remyelinate and restore locomotion after spinal cord injury. *J Neurosci* 25: 4694 – 4705

Kim JB, Zaehres H, Wu G, Gentile L, Ko K, Sebastiano V, Araúzo-Bravo MJ, Ruau D, Han DW, Zenke M, Schöler HR (2008) Pluripotent stem cells induced from adult neural stem cells by reprogramming with two factors. *Nature* 454: 646 – 650

Kim JB, Greber B, Arauzo-Bravo MJ, Meyer J, Park KI, Zaehres H, Scholer HR (2009a) Direct reprogramming of human neural stem cells by OCT4. *Nature* 461: 649 – 653

Kim JB, Sebastiano V, Wu G, Araúzo-Bravo MJ, Sasse P, Gentile L, Ko K, Ruau D, Ehrich M, van den Boom D, Meyer J, Hübner K, Bernemann C, Ortmeier C, Zenke M, Fleischmann BK, Zaehres H, Schöler HR (2009b) Oct4-induced pluripotency in adult neural stem cells. *Cell* 136: 411 – 419

Kim JB, Zaehres H, Arauzo-Bravo MJ, Scholer HR (2009c) Generation of induced pluripotent stem cells from neural stem cells. *Nat Protoc* 4: 1464 – 1470

Kim J, Efe JA, Zhu S, Talantova M, Yuan X, Wang S, Lipton SA, Zhang K, Ding S (2011) Direct reprogramming of mouse fibroblasts to neural progenitors. *Proc Natl Acad Sci USA* 108: 7838 – 7843

Lee BB, Cripps RA, Fitzharris M, Wing PC (2014) The global map for traumatic spinal cord injury epidemiology: update 2011, global incidence rate. *Spinal Cord* 52: 110 – 116

Lee JH, Mitchell RR, McNicol JD, Shapovalova Z, Laronde S, Tanasijevic B, Milsom C, Casado F, Fiebig-Comyn A, Collins TJ, Singh KK, Bhatia M (2015) Single transcription factor conversion of human blood fate to NPCs with CNS and PNS developmental capacity. *Cell Rep* 11: 1367 – 1376

Li J, Huang NF, Zou J, Laurent TJ, Lee JC, Okogbaa J, Cooke JP, Ding S (2013) Conversion of human fibroblasts to functional endothelial cells by defined factors. *Arterioscler Thromb Vasc Biol* 33: 1366 – 1375

Mitchell R, Szabo E, Shapovalova Z, Aslostovar L, Makondo K, Bhatia M (2014a) Molecular evidence for OCT4-induced plasticity in adult human fibroblasts required for direct cell fate conversion to lineage specific progenitors. *Stem Cells* 32: 2178 – 2187

Mitchell RR, Szabo E, Benoit YD, Case DT, Mechael R, Alamilla J, Lee JH, Fiebig-Comyn A, Gillespie DC, Bhatia M (2014b) Activation of neural cell fate programs toward direct conversion of adult human fibroblasts into tri-potent neural progenitors using OCT-4. *Stem Cells Dev* 23: 1937 – 1946

Miura K, Okada Y, Aoi T, Okada A, Takahashi K, Okita K, Nakagawa M, Koyanagi M, Tanabe K, Ohnuki M, Ogawa D, Ikeda E, Okano H, Yamanaka S (2009) Variation in the safety of induced pluripotent stem cell lines. *Nat Biotech* 27: 743 – 745

Morita R, Suzuki M, Kasahara H, Shimizu N, Shichita T, Sekiya T, Kimura A, Sasaki K, Yasukawa H, Yoshimura A (2015) ETS transcription factor ETV2 directly converts human fibroblasts into functional endothelial cells. *Proc Natl Acad Sci USA* 112: 160 – 165

Najm FJ, Zaremba A, Caprariello AV, Nayak S, Freundt EC, Scacheri PC, Miller RH, Tesar PJ (2011) Rapid and robust generation of functional oligodendrocyte progenitor cells from epiblast stem cells. *Nat Methods* 8: 957 – 962

Najm FJ, Lager AM, Zaremba A, Wyatt K, Caprariello AV, Factor DC, Karl RT, Maeda T, Miller RH, Tesar PJ (2013) Transcription factor-mediated reprogramming of fibroblasts to expandable, myelinogenic oligodendrocyte progenitor cells. *Nat Biotech* 31: 426 – 433

Nakae A, Nakai K, Yano K, Hosokawa K, Shibata M, Mashimo T (2011) The animal model of spinal cord injury as an experimental pain model. *J Biomed Biotechnol* 2011: 939023

Noble M, Murray K, Stroobant P, Waterfield MD, Riddle P (1988) Platelet-derived growth factor promotes division and motility and inhibits premature differentiation of the oligodendrocyte/type-2 astrocyte progenitor cell. *Nature* 333: 560 – 562

Noll E, Miller RH (1993) Oligodendrocyte precursors originate at the ventral ventricular zone dorsal to the ventral midline region in the embryonic rat spinal cord. *Development* 118: 563 – 573

Raff MC, Lillien LE, Richardson WD, Burne JF, Noble MD (1988) Platelet-derived growth factor from astrocytes drives the clock that times oligodendrocyte development in culture. *Nature* 333: 562 – 565

Richardson WD, Pringle N, Mosley MJ, Westermark B, Dubois-Dalcg M (1988) A role for platelet-derived growth factor in normal gliogenesis in the central nervous system. *Cell* 53: 309 – 319

Sekiya S, Suzuki A (2011) Direct conversion of mouse fibroblasts to hepatocyte-like cells by defined factors. *Nature* 475: 390 – 393

Sharp J, Frame J, Siegenthaler M, Nistor G, Keirstead HS (2010) Human embryonic stem cell-derived oligodendrocyte progenitor cell transplants improve recovery after cervical spinal cord injury. *Stem Cells* 28: 152 – 163

Silva NA, Sousa N, Reis RL, Salgado AJ (2014) From basics to clinical: a comprehensive review on spinal cord injury. *Prog Neurobiol* 114: 25 – 57

Sim FJ, McClain CR, Schanz SJ, Protack TL, Windrem MS, Goldman SA (2011) CD140a identifies a population of highly myelinogenic, migration-competent and efficiently engrafting human oligodendrocyte progenitor cells. *Nat Biotechnol* 29: 934 – 941

Szabo E, Rampalli S, Risueno RM, Schnerch A, Mitchell R, Fiebig-Comyn A, Levadoux-Martin M, Bhatia M (2010) Direct conversion of human fibroblasts to multilineage blood progenitors. *Nature* 468: 521 – 526

Talac R, Friedman JA, Moore MJ, Lu L, Jabbari E, Windebank AJ, Currier BL, Yaszemski MJ (2004) Animal models of spinal cord injury for evaluation of tissue engineering treatment strategies. *Biomaterials* 25: 1505 – 1510

Wang S, Bates J, Li X, Schanz S, Chandler-Militello D, Levine C, Maherali N, Studer L, Hochedlinger K, Windrem M, Goldman Steven A (2013) Human iPSC-derived oligodendrocyte progenitor cells can myelinate and rescue a mouse model of congenital hypomyelination. *Cell Stem Cell* 12: 252 – 264

Warlich E, Kuehle J, Cantz T, Brugman MH, Maetzig T, Galla M, Filipczyk AA, Halle S, Klump H, Scholer HR, Baum C, Schroeder T, Schambach A (2011) Lentiviral vector design and imaging approaches to visualize the early stages of cellular reprogramming. *Mol Ther* 19: 782 – 789

Wernig M, Meissner A, Foreman R, Brambrink T, Ku M, Hochedlinger K, Bernstein BE, Jaenisch R (2007) *In vitro* reprogramming of fibroblasts into a pluripotent ES-cell-like state. *Nature* 448: 318 – 324

Xu J, Du Y, Deng H (2015) Direct lineage reprogramming: strategies, mechanisms, and applications. *Cell Stem Cell* 16: 119 – 134

Yang N, Zuchero JB, Ahlenius H, Marro S, Ng YH, Vierbuchen T, Hawkins JS, Geissler R, Barres BA, Wernig M (2013) Generation of oligodendroglial cells by direct lineage conversion. *Nat Biotech* 31: 434 – 439

Zaehres H, Daley GQ (2006) Transgene expression and RNA interference in embryonic stem cells. *Methods Enzymol* 420: 49 – 64